Lehrstuhl für Bildverarbeitung
Institute of Imaging & Computer Vision

Automatic measuring of quality criteria for heart valves

Alexandru P. Condurache and Tobias Hahn and Ulrich G. Hofmann and Michael Scharfschwerdt and Martin Misfeld and Til Aach

Institute of Imaging and Computer Vision
RWTH Aachen University, 52056 Aachen, Germany
tel: +49 241 80 27860, fax: +49 241 80 22200
web: www.lfb.rwth-aachen.de

in: SPIE Medical Imaging 2007, Image Processing. See also BibTeX entry below.

BibTeX:

```
@inproceedings{CON07a,
  author    = {Alexandru P. Condurache and Tobias Hahn and
               Ulrich G. Hofmann and Michael Scharfschwerdt and
               Martin Misfeld and Til Aach},
  title     = {Automatic measuring of quality criteria for heart valves},
  booktitle = {SPIE Medical Imaging 2007, Image Processing},
  publisher = {SPIE},
  year      = 2007,
  pages     = {in print},
}
```


document created on: February 15, 2007
created from file: CON07a.tex
cover page automatically created with CoverPage.sty
(available at your favourite CTAN mirror)

RWTH AACHEN
RHEINISCH-WESTFÄLISCHE TECHNISCHE HOCHSCHULE AACHEN

Automatic measuring of quality criteria for heart valves

Alexandru Paul Condurache[a], Tobias Hahn[a], Ulrich G. Hofmann[a], Michael Scharfschwerdt[b], Martin Misfeld[b] and Til Aach[c]

[a]Institute for Signal Processing, University of Luebeck, Ratzeburger Allee 160, 23538 Luebeck, Germany;
[b]Clinic for Heart Surgery, University Clinic Schleswig-Holstein, Ratzeburger Allee 160, 23538 Luebeck, Germany;
[c] Institute of Imaging and Computer Vision, RWTH-Aachen University, Templergraben 55, 52056 Aachen, Germany

ABSTRACT

Patients suffering from a heart valve deficiency are often treated by replacing the valve with an artificial or biological implant. In case of biological implants, the use of porcine heart valves is common. Quality assessment and inspection methods are mandatory to supply the patients (and also medical research) with only the best such xenograft implants thus reducing the number of follow-up surgeries to replace worn-up valves. We describe an approach for automatic in-vitro evaluation of prosthetic heart valves in an artificial circulation system. We show how to measure the orifice area during a heart cycle to obtain an orifice curve. Different quality parameters are then estimated on such curves.

Keywords: prosthetic heart valves, quality control, valve-orifice area, thresholding, snake

1. INTRODUCTION

Replacing a deficient heart valve with a xenograft implant is a common procedure in cardiac surgery.[1] Porcine heart valves are preferred for this procedure because of their similarity to the human heart valve and the easy access to these valves. Typically a large number of porcine valves are available from specially bread animals. Therefore, quality assessment becomes a vital task to provide patients, surgeons and researchers with the most suitable material. Major quality criteria are the maximum value of the orifice area and the evolution of this area over a valve cycle – i.e. the time interval between the moment the valve opens until it closes. Although there are already approaches to determine the valve-orifice area automatically,[2] this is still done manually in most cases. In either case a sequence of images showing a valve cycle is used. The images are acquired with the help of a test setup. A human operator has to select a set of points at the leaflets tips and connections to define six triangles. Summed areas give an approximation to the orifice area. This approximation neglects the rather curved boundary of the leaflets. Also the area is measured in only a few images of the sequence and from there, orifice curves – i.e. curves of area over frame index, showing the behavior of the valve over a cycle – are interpolated. The methods described in this contribution are intended to provide the researcher with a more precise, reproducible and robust technique to calculate the orifice area automatically. We first segment the orifice and then compute its area by counting all object pixels. To obtain an orifice curve, segmentation of all images in an analyzed sequence is done by a combination of threshold- and snake-based methods.

1.1. Data acquisition

The area of the valve orifice is measured in each of a sequence of images acquired in vitro in a special test setup,[3] which is shown in Figure 1 (a) and (b). From a reservoir (1) a transparent fluid – usually sterile water – is transported through a disc valve (4) by a piston pump (2), which is driven by a waveform adapted cam plate (3). After passing an input compliance (5) the fluid is pressed through the inspected heart valve (11) into a visualization chamber (7) located in another fluid reservoir (6). Pressure sensors (10) are installed below and

A.P.C. and T.H. contributed equally. Send correspondence to A.P.C.: E-mail: condura@isip.uni-luebeck.de, Telephone: +49 (0)451 500 5801

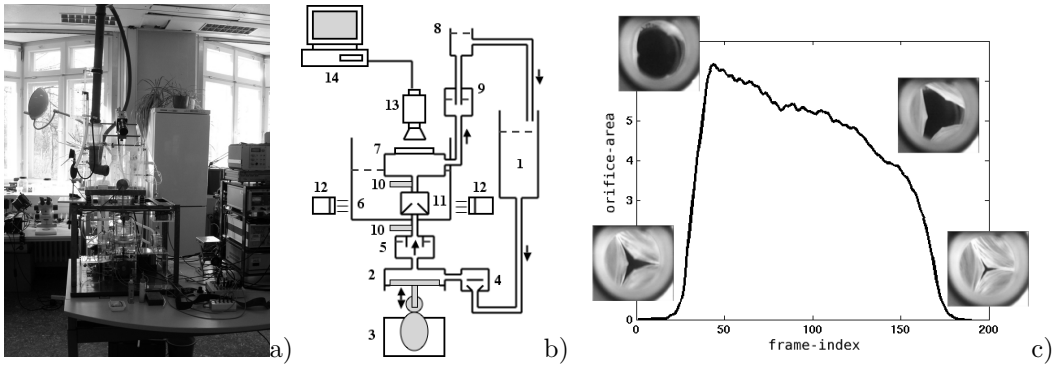

Figure 1. Experimental setup (a), its schematics (b) and an orifice curve (c).

above the heart valve. Passing an aortic compliance (9) the fluid reaches a height variable column and flows back to the first reservoir. The heart valve is illuminated by light sources (12) outside the fluid tank (6) made from perspex. A high-speed video camera (13) takes images of the heart valve. The inspected valve is mounted inside a tube. The portion of the tube before the valve with respect to the camera is protected from light, such that when the valve opens the orifice appears dark, while the valve itself is light as it receives illumination. The digitized images are stored on a PC (14).

Images of the heart valve are taken with 500 fps and an interlaced resolution of 480x420 gray pixels. A test sequence (see Figure 1 (c)), which shows one valve cycle, has a duration of some half a second, leading to approximatively 250 frames per sequence. Imaging by an interlaced camera introduces artefacts on moving objects. In this case, such artefacts can be observed on the margins of the leaflets. Illumination is provided by Neon-lamps. Such an illumination modality introduces also artefacts, as the 60 Hz flickering of the lamp is observable in the 500 Hz image sequence.

The sequences we analyzed were acquired with the test-bed described above. Therefore, they show interlace- and illumination-related artefacts. Clearly, such problems can be avoided by improving the test environment, such that it uses a progressive-scan camera and a continuous light-source for illumination. To suppress interlace-related artefacts we apply an opening operation with a disk-like structuring element of small size. To reduce the influence of the flickering, for each image a value is added or subtracted such that the mean gray-level value in a manually-chosen region – which under continuous illumination should have constant gray-levels – remains constant over the entire sequence.

2. METHODS

To obtain orifice-area curves, one needs to segment the dark orifice from its light background in each image of a test sequence. We describe two classes of methods for the segmentation of the orifice: (i) thresholding-based methods (see Section 2.1) and (ii) active contour-based methods (see Section 2.2). From each analyzed image-sequence we obtain one orifice curve (see Section 2.3), which can then be used to judge the quality of the inspected valve.

2.1. Segmentation of the orifice area by thresholding

Besides the valve, each image of a test sequence shows also parts of the tube through which the water flows and some of the area outside this tube. The tube appears similar to the valve and the area outside the tube similar to the orifice (see Figure 2 (a)). To focus our analysis on the valve alone, we establish a *valve-ROI* (see Figure 2 (c)) and ignore the rest of the image. Since on each analyzed image we expect to see only two pixel classes, i.e., orifice and non-orifice/valve, the straightforward method to segment the orifice is by gray-level thresholding.[1] Thresholding can still be used if the underlying model is no longer *bi-class* but *multi-class*. In this case one has to use the prior information that the orifice gray-levels are the darkest ones in the valve-ROI.

Figure 2. Original image (a), edge detection result (b) and Hough-segmented outline (c)

In general, one can either threshold each image individually, or establish one global threshold for an entire sequence. As we do not expect to observe an orifice in each of the analyzed images, a global threshold is better suited.

2.1.1. Establishing a valve-ROI

The camera observes the valve trough the tube, using a normal-imaging optical system. Thus, the inner wall of the tube is also observable and delineates the contour of the valve. We use this circular outline as a mask and ignore everything outside it.

We segment the circular outline by the Hough transform for circles.[4,5] As the approximate position of the center of this circle and the size of its radius are known a priori, the search in the Hough-space is very fast. We search the coordinates of the center in a ROI of size 15 pixels centered at the image center and the radius on an interval of the same size centered at the value 150. The center and radius of the outline circle is then estimated by taking the mean over several images in the beginning of the analyzed sequence. This defines a circular ROI where only the valve is visible. An example is shown in Figure 2 .

2.1.2. Thresholding with a bi-class model

Using the global histogram of a sequence, which is computed from the gray-levels of all images, the threshold can be established either manually by the user or automatically.

Manual thresholding by the user, is done by trial and error. Clearly, this makes the procedure tedious and the results rarely reproducible. An automatic procedure can avoid such drawbacks. Assuming that only two pixel classes are observable in the analyzed sequences, we set a global threshold automatically by the Otsu-method,[6] which finds the threshold by optimizing a measure of separability on the analyzed histogram.

In some sequences the results achieved by a global threshold include relatively often other image structures besides the orifice, e.g., parts of a leaflet, as shown in Figure 3 (b). These artefacts are usually unconnected to the orifice and can be eliminated from the segmentation in a *postprocessing* step.

Postprocessing. We know that the orifice is a connected structure. As the valve is imaged in a centered position and thus the image center will be practically always contained within the orifice, we use the center-pixels – i.e. the pixels situated in a circle of radius five pixels centered at the image center – to select from the initial raw segmentation only those connected structures containing at least one of them.[7] A circle is used to account for the variability in the positioning of the valve. This is shown in Figure 3. The initial thresholding result contains more structures besides the orifice (Figure 3 (b)). After center-based selection, only the orifice remains (Figure 3 (c)).

2.1.3. Thresholding with a multi-class model

Global thresholding followed by postprocessing will fail if spurious structures are linked to the orifice. Such an example is shown in Figure 4 (b). Such over-segmentations show that our initial assumption, having only two pixel-classes in the analyzed images, is sometimes incorrect and there are actually *several classes present*. However, one can usually safely assume the darkest pixels in the valve-ROI to be orifice pixels. Therefore, if we use a *mixture model* of the global-histogram, to *segment the orifice* we have to separate the mode with the darkest mean gray-level from the rest.

Figure 3. Valve image (a), thresholding result (b), and final result after center-based selection (c).

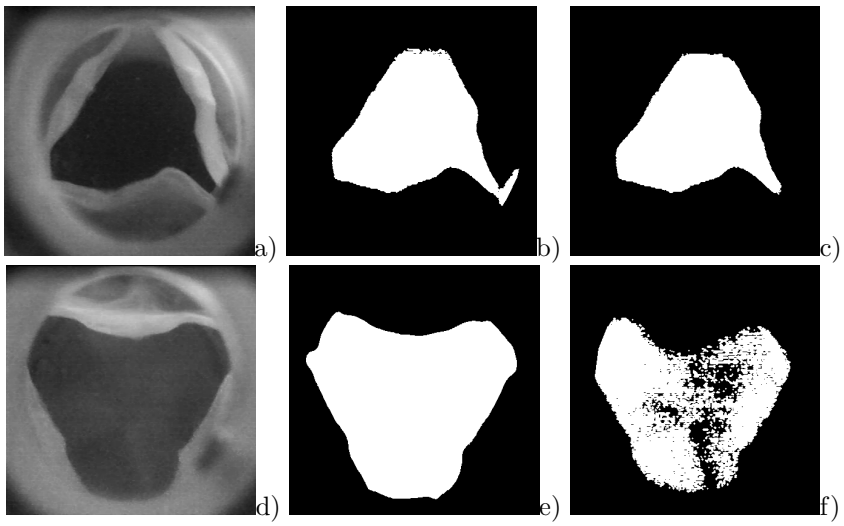

Figure 4. Original image (a), (d) segmentation result by the Otsu-method (b), by the FMM-method (c), (f) and by snakes (e).

Finite mixture-models. We would like thus to model a multi-modal histogram and select the darkest mode. We know a priori neither the number of modes nor the type of the mixture. To proceed, one can assume a certain type of mixture (e.g. Gaussian) and determine its parameters by the EM algorithm.[8–10] One needs to determine also the optimal number of modes k. The maximized likelihood cannot be used directly for this purpose because it is a nondecreasing function of k.[11] However, one can proceed by trying several values and choosing then the best suited one according to coding-theory-based mixture criteria such as: the minimum message length (MML),[12,13] the minimum description length (MDL),[14,15] Akaike's information criterion[16] and others.[17] There are also other criteria to find k, but which are less popular (see 18 and the references therein).

With respect to the way the optimal mixture decomposition is found, this approach has the disadvantage that each candidate mixture has first to be estimated by the EM algorithm, which is sensible to the initialization and whose convergence is difficult – in particular if the number of modes is larger than the true one.

Alternatively, it has been proposed to directly optimize a mixture-criterion via EM. For this purpose, a modified MML criterion is used. The algorithm thus obtained is called the Finite Mixture Model (FMM) and it was first proposed in Reference [18].

This algorithm is less initialization-dependent and shows a better convergence.[18] We justify the modeling by a Gaussian mixture with the prior knowledge that the orifice is characterized by similar gray-levels in each sequence, with some deviations from the expected orifice gray-level generated by varying illumination conditions. The same is valid for all other objects present in the analyzed images.

Segmentation of the orifice. After computing the optimal mixture-model, the threshold is found by a likelihood ratio test[19] using the two mixture components with the smallest means – thus separating the darkest

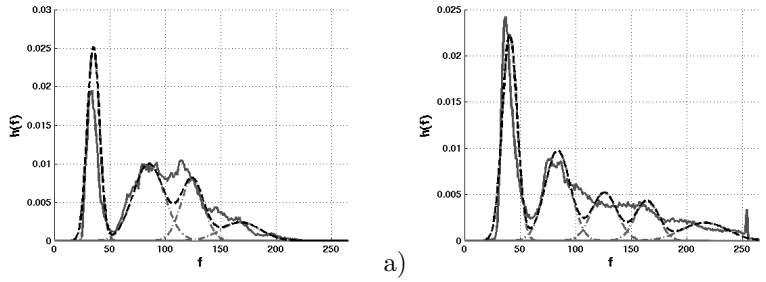

Figure 5. Outline of the normalized global-histogram (continuous line), estimated mixture (dashed line) and estimated mixture components (dashed-dotted line) for two sequences from our data-base. The threshold to segment the orifice is set such as to separate the darkest mode from the next darkest.

mode from the rest, as orifice pixels have the smallest gray-levels in the analyzed circular ROI. This is then practically identical to the overall optimum, as the conditional probabilities of other mixture models around the threshold are always close to zero. This is shown for two examples in Figure 5.

When using the mixture-decomposition method, the over-segmentation is no longer an issue in the segmentation of the orifice of a heart-valve (see Figure 4 (f)). Consequently, there is no need for center-based selection anymore. However, in some cases under-segmentation becomes now an issue. Such an example is shown in Figure 4 (f).

2.2. Snake-based segmentation of the orifice area

Threshold-based methods may fail because the orifice does not have a homogeneous gray-level representation, as it is not defined over a certain reflectivity – which can be then translated into an own gray-level distribution – but it is defined by the borders of the leaflets. The orifice is actually transparent and it will thus take over the gray-level of the structures against which it is imaged. Practice shows that it is rather difficult to achieve a homogeneous background to project the orifice against.

For a better segmentation one should thus start from the leaflets and select the orifice as defined by their borders, i.e., as the area enclosed within these borders. The border-shape curves cannot be described a priori as they have a large variability. Therefore, we use snakes,[20] which are well suited to track them over the analyzed sequence.[21] As external force we use a Gradient Vector Flow (GVF),[22,23] which has an improved attraction range in comparison to other external forces.[24]

The snake is *initialized* automatically after the valve has opened sufficiently to see the orifice. We initialize the snake from the leaflet base-lines, which are the lines connecting each of the *anchor points*. Anchor points are the points where two leaflets meet (see Figure 8 (f)). After initialization, the snake will *track the outline of the leaflets* (see e.g. Figure 7 (d)) until the valve closes.

2.2.1. Initialization

The snake can track the outlines of the leaflets only in images where these are well observable. Therefore, for a successful initialization one has to wait for the valve to open sufficiently and then halt the snake at the end of the sequence, when the opening is no longer large enough. To reduce the time interval since the moment when the valve opens until the snake is initialized, we use a balloon pressure force[25] to push the base line toward the borders of the leaflets. However, such a balloon has to be carefully parameterized to avoid a collapse of the snake. After the base line initialization, the position of the snake in the previous image is used as initialization for the current image.

Initialization from the base line has the additional advantage of placing snakels already in regions where the borders of the leaflets are not well defined, e.g., they are imaged against parts of the tube seen through the orifice. This is shown in Figure 4 (a) – see the vicinity of the upper anchor point.

To find out when to initialize the snake, we follow the mean-value of the gray-levels within a circle, defined such that it is maximally enclosed in the triangle given by the base lines. If this value drops beneath a certain

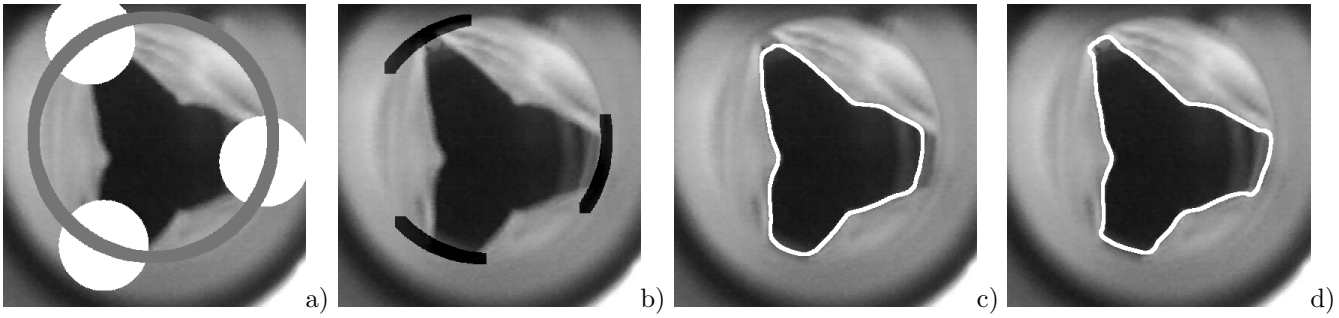

Figure 6. Construction of attractors (a) and final result (b). Snake segmentation result without (c) and with (d) attractor.

threshold, then we conclude that the valve has opened and initialize the snake. The threshold is chosen as the median of the center mean-values recorded over the first 25 frames of a sequence. At the end of the sequence, if the mean value is above the threshold, the snake-based tracking is aborted.

2.2.2. Snakes-based tracking of the leaflet border

After the snake has converged in the initialization frame, its position in the past image is used as initialization for the next one and so on. To avoid a collapse of the snake, it tracks the leaflets until shortly before the valve closes. The GVF is used as external force field, conferring robustness to the segmentation through its improved attraction range and concavity behavior.[23]

During tracking the snake cannot follow the valve orifice in regions of small contrast, i.e., where portions of the tube behind the valve are visible through the opening. This is shown in Figure 6 (e). The usual solution for solving such convergence problems, is to use a balloon pointing outwards from the image center. A balloon approach is problematic when the valve starts closing. It may happen that due to the balloon the snake loses the orifice. This will lead to a complete failure of the analysis, due to the way the snake is initialized, i.e., from the previous frame. Initializing the snake each time from a small circle centered at the image center has the potential to solve such problems at least partially, as in this case the tracking will fail only for single frames. Generally, balloons need to be used very carefully and usually only when the sought features are strong enough to yield a good attraction basin. As balloons are unsuited, we show how to build *attractors* for the snake around the *anchor points*, such that the snake tracks the borders of the leaflets correctly, as in the example shown in Figure 6 (d).

Anchor-points-based attractors for better tracking. To build artificial attractors around the anchor points, we use the circular outline, which was segmented during initialization. The artificial attractors are actually edges, constructed from parts of the circular outline in the vicinity of anchor points. These vicinities are circular in shape and have a radius of 125 pixels.

To begin with, the circular outline is dilated slightly, starting from its initial one pixel width, to increase its attraction range. Then, parts of the outline around each anchor point are selected. The selection includes those parts found in a circle of radius 125 pixels around each anchor point. Finally, they are subtracted from the original image such that their mean gray-level is equal to the mean gray-level in the dark parts of the orifice. An example is shown in Figure 6 (a) and (b).

We do not use the entire circular outline as one attractor, because such a strategy may lead to failure, e.g., if one of the leaflets can no longer be observed as it travels behind the circular-outline, then the snake will reach and possibly remain there even if the valve starts closing. Such an example is shown in Figure 7.

2.2.3. Automatic determination of the anchor points

The anchor points are needed during initialization to define the base lines, but also during tracking to build the attraction basins which constrain it. Anchor points are established automatically. For this purpose, we use the first 11 frames after the valve has opened, i.e., before the valve is completely opened. For these images we

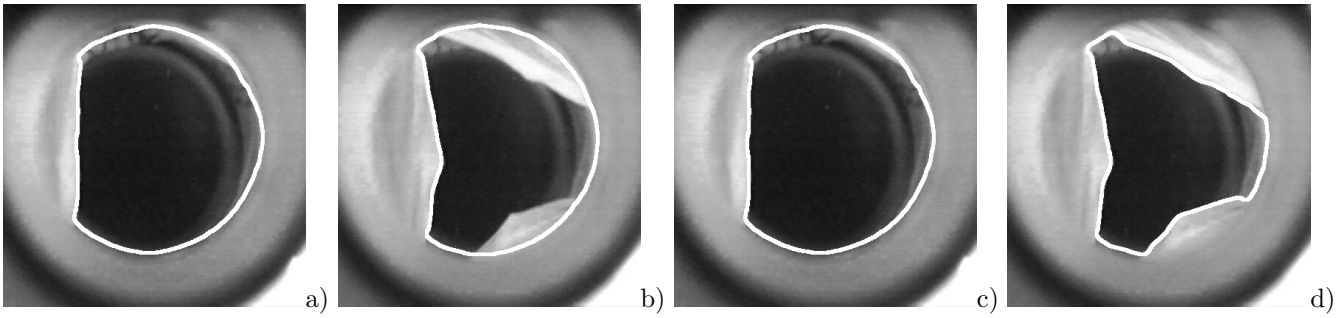

Figure 7. Snake result for two frames using the entire circular outline as attractor (a) and (b) and the same images using only the portions of the circular outline around the anchor points as attractor (c) and (d).

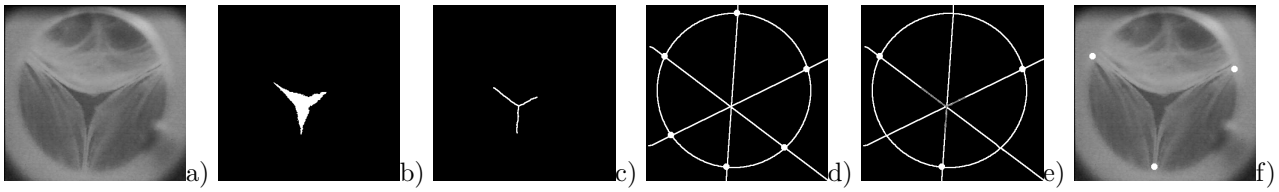

Figure 8. Automatic anchor points detection. Original image (a), segmented orifice (b), result of morphological processing (c), intersection of centerline-rays with the outline of the valve-ROI (d), minimum-distance points (e) and final result (f).

can safely assume that the orifice has a homogeneous and unique gray-level representation and segment it by thresholding. One such example is shown in Figure 8 (b).

We start by segmenting the circular outline. We then find the center-lines of the orifice by dilating and then thinning the segmentation result (see Figure 8 (c)). The dilation is necessary to ensure that only the centerline remain after thinning. Then, we use the Hough transform for lines to detect the three center-line rays and compute the points where these rays intersect the circular outline (see Figure 8 (d)). Subsequently, distances from the intersection point to all center-line points along the ray are computed, for each ray and for every point where it intersects the circular outline. For each intersection point only the minimum is considered. Anchor point is then the intersection point with the minimum value (see Figure 8 (e)). The final positions of the anchor points are determined by taking the mean position over 11 frames for each anchor point. This is shown in Figure 8 (f).

2.3. Practical computation of orifice curves and data analysis

To analyze an entire sequence, we propose to use a global threshold to segment the orifice in those images in the beginning and the end of a sequence, when the snake cannot be properly defined. One can be reasonably certain that a gray-level threshold segments the orifice properly, because then it can be safely assumed that the orifice, due to its small size, is imaged against an uniform-background . Even if in some rare cases the threshold can fail, most of the sequence will be correctly segmented nevertheless by the snake, as this is initialized from the leaflet baseline and not based on the result achieved by the threshold. Using this combination between gray-level threshold and snake, we successfully segment the orifice over an entire valve cycle. We propose to use the multi-class-model threshold for those images where the snake does not function properly.

There are two quality criteria which can be measured on such curves. First is the maximum-value and then the dynamic evolution of the orifice-area. For a healthy valve, the maximum value has to be within a certain predefined interval, such that a proper blood flow is obtained without additional stress for the heart. With respect to the dynamic evolution, a valve cycle has to show three phases and the orifice curve of a healthy valve should accordingly show three regions. The first phase is the rapid increase phase, when the orifice increases rapidly to its maximum value as the valve is opening, during the second phase, the area of the orifice should decrease slowly, the valve being now opened and finally in the third phase, the area decreases sharply and the

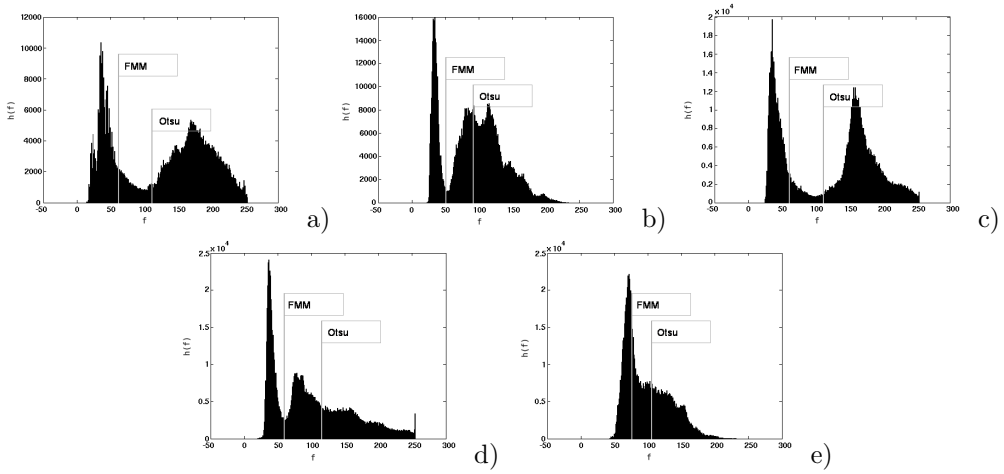

Figure 9. Global histogram and thresholds for five different sequences.

valve closes completely. Such a typical behavior is shown Figure 11 (a). Also, during one valve cycle, the values of the orifice area in each phase have to fall into certain predefined intervals.

The dynamic behavior of the valve during the three phases can be measured by the derivative of the curve in each region. The three orifice-curve regions corresponding to the three phases of the valve cycle are segmented as with the methods used to select the complete state in Reference [26].

3. EXPERIMENTS AND DISCUSSION

To determine the orifice area of the valve, we have followed a threshold-based and a snake-based approach. Within the first approach, to find the orifice area we compare each image to an adaptively determined threshold. We have investigated two automatic thresholds: the first one assumes a bi-class model of the global histogram and sets the threshold by the Otsu-method and the second, assumes a multi-class model and finds the threshold by a likelihood ratio test between the two darkest components of a mixture whose parameters are found using the FMM (see Figure 9). The second approach is based on an appropriately designed snake. The orifice area is obtained as the area enclosed by the snake. We have improved the external energy term such that the snake follows the leaflet everywhere.

In Figure 11 orifice-area curves plotted over time-index for each of the sequences in the data-base and by each method are shown. The results for the Otsu-threshold have been achieved with center-selection and the results for the mixture decomposition without.

Threshold-based methods. The Otsu-threshold is usually larger than the mixture-threshold. This has the disadvantage of returning over-segmentations (see the spikes in Figure 11 (d)), but at the same time it makes it less sensible to illumination variations (see the ripples in figure 11 (a)). In many cases the over segmentation problem of the Otsu-threshold can be solved by center-based selection and it usually affects only some images in a sequence.

The FMM-threshold returns better results from the point of view of a classification algorithm, since it separates better the darkest cluster on the global-histogram for each sequence. This is shown in Figure 9. It appears however, that the mixture-threshold is actually too conservative for some sequences. The reason for this is that the orifice gray-levels do not cluster well, or in other words the orifice surface does not contain a single type of dark pixels. This is due, e.g., to the light coming sideways to the valve and making thus some orifice parts lighter than others (see Figure 10 (b) and (c)), but also to the fact that reflections appear. It may even occur that small parts from the test-setup tube below the valve appear in the orifice. This happens particularly when the valve is fully-opened (see Figure 10 (a)). If the FMM-method fails, then it will be likely to fail for an entire sequence (see Figure 11 (e)).

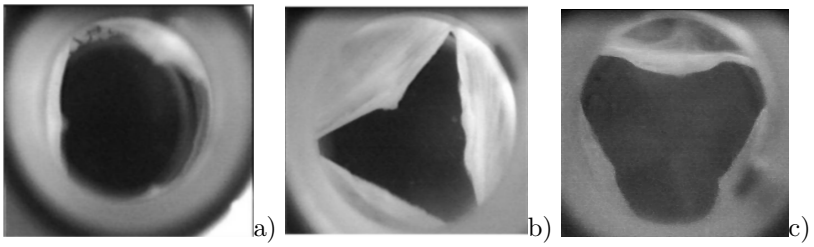

Figure 10. Examples from sequences where the valves show an inhomogeneous orifice.

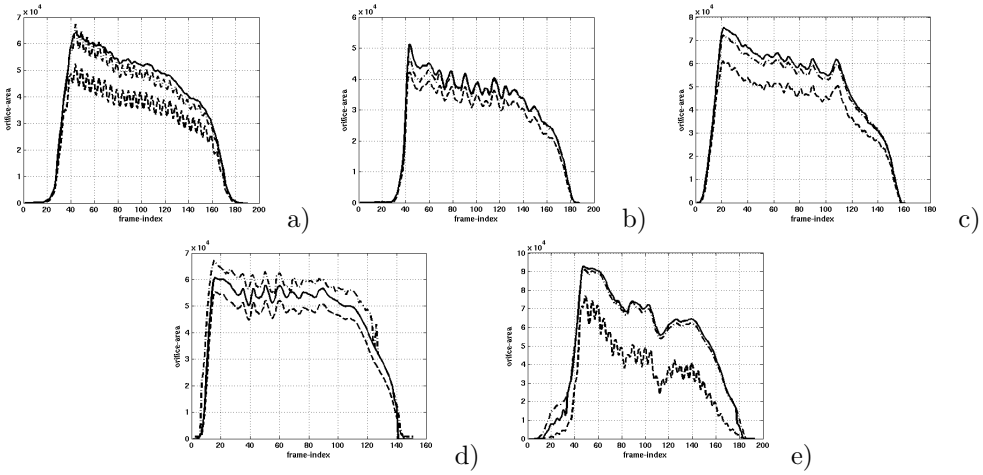

Figure 11. Orifice curves computed by different methods: using snakes (continuous line), the Otsu-threshold (dashed-dotted line) and the FMM-threshold (dashed line).

Snake-based tracking of the orifice border. The assumption that an orifice is darker than its background holds practically always. However, the orifice and background are in many cases not perfectly homogeneous (see Figure 10). Also, all five sequences used here to test the proposed algorithms, which have been acquired with the currently available test setup, are affected by illumination variations.

Snakes are robust against illumination variations and offer good orifice segmentation results, as long as the edges they follow are still distinguishable, irrespective if the orifice and/or background are homogeneous or not. They are also able to follow the leaflet border even in regions where the contrast between the leaflet and the background is weak and are thus superior to threshold-based approaches, as shown also in Figures 4 (e) and 11. The orifice curves computed by snakes usually show neither ripples nor spikes and return results in good agreement with the expectations of human experts.

The result of the segmentation depends on the attraction range of the external energy and also on the way the energy is defined around the anchor points. A GVF offers a large attraction range and good convergence in regions of high border-curvature.[23] The attractors make sure that the external-energy field converges properly around anchor points.

Because images are acquired at high frame-rate, the distance traveled by the leaflets between two consecutive images is small enough such that the converged snake from the previous image is practically always in the attraction sink of the leaflet borders in the current image.

Comparison between methods. Comparing the two automatic thresholds with respect to how good they segment the orifice, it seems that the Otsu-threshold functions better for some sequences (e.g. the one shown in Figure 11 (e)) and the FMM-threshold for others (e.g. the one shown in Figure 11 (d)). The FMM-threshold returns better results from the point of view of a classification algorithm. It separates better the darkest dome of the global-histogram, which is usually associated with the orifice (see Figure 9). This however is not always

enough in practice, due to the inhomogeneity of the gray-level representation of the orifice. The FMM-threshold is usually too conservative.

Apart from the fact that they have to be initialized when the valve has already opened and can not follow it up until this is completely closed, active contours with GVF for the external-energy term are well suited for the segmentation of the valve orifice. The extended energy term, with attractors near the anchor points, ensures a precise segmentation of the valve border over its entire length. They give better, more robust results than thresholds. This is particularly true for the sequences from our data base, which have been recorded using a flickering illumination source. As shown, e.g., in Figure 11 (a) and Figure 11 (d) the threshold-based orifice curves, as opposed to the snake-based ones, capture also the flickering, which in turn can be misinterpreted for fluttering of the leaflets.

4. CONCLUSIONS

We have described methods for the automatic computation of quality measures for heart valves. We expect the automatic measuring of the orifice area to improve on the current methods mainly in two ways, besides improved reproducibility of the obtained results:

1. **More precise**, because usually humans are prone to errors while performing such painstaking jobs. Also, during manual analysis only a few images from the available sequence are actually analyzed and the sought measures are then computed from data interpolated from these measurements. Automatic measurements use all images in the sequence.
2. **Faster**, such that more implants can be inspected and the chances of finding a better one rise.

The orifice curve describes the evolution of the area of the orifice during a valve cycle. This should exhibit a specific form – showing all three typical phases: rapid-increase, slow-decrease, fast-decrease – which permits then the calculation of features linked to the dynamic properties of the heart valve as, e.g., opening and closing speed. Also, the values of the area of the orifice during each phase and in particular the maximal value, has to fall in a certain interval.

We have applied these methods to the quantification of the quality of heart valves with three leaflets. This category includes the aortic, the pulmonary and the tricuspid valves. However, we believe that such methods can be also successfully used for bicuspid valves, thus constituting a tool for heart valves analysis in general.

Orifice curves are obtained from the evolution of the segmented area of the orifice over the frame index. We consider that the snake-based computation of the orifice area is the most appropriate method. The disadvantages of the snakes are that practically they need to be initialized after the valve has opened and can not follow the orifice until the valve is completely closed. Therefore, we propose a combination of threshold and snake methods to compute an orifice curve. The threshold is used for those images, in the beginning and end of a sequence, where the snake would fail.

REFERENCES

1. T. Hahn, A. P. Condurache, T. Aach, M. Scharfschwerdt, and M. Misfeld, "Automatic in-vitro orifice area determination and fluttering analysis for tricuspid heart-valves.," in *Proceedings of BVM-2006*, pp. 21–25, Springer, (Hamburg, Germany), May 19–21 2006.
2. R.-U. Kuehnel, A. Pohl, R. Puchner, M. O. Wendt, M. Hartrumpf, M. Pohl, and J.-M. Albes, "Opening and closure characteristics of different types of stented biological valves," *The Journal of Thoracic and Cardiovascular Surgery* **54**, pp. 85–90, 2006.
3. M. Scharfschwerdt, M. Misfeld, and H.-H. Sievers, "The influence of a nonlinear resistance element upon in-vitro aortic pressure tracings and aortic valve motions," *American Society for Artificial Internal Organs* **50**(5), pp. 498–502, 2004.
4. P. V. C. Hough, "Methods and means for recognizing complex patterns.," in *US patent nr. 3069654*, 1962.
5. J. Illingworth and J. Kittler, "A survey of the Hough transform.," *Computer Vision Graphics and Image Processing* **44**(1), pp. 87–116, 1988.

6. N. Otsu, "A threshold selection method from gray-level histograms.," *IEEE Transactions on Systems, Man and Cybernetics* **SMC-9**(1), pp. 62–66, 1979.
7. A. P. Condurache and T. Aach, "Vessel segmentation in 2D-projection images using a supervised linear hysteresis classifier.," in *Proceedings of ICPR-2006*, **1**, pp. 239–243, IEEE, (Hong Kong, China), August 20–24 2006.
8. A. P. Dempster, N. M. Laird, and D. B. Rubin, "Maximum likelihood from incomplete data via the em algorithm.," *Journal of the Royal Statistical Society* **B**(39), pp. 1–38, 1977.
9. J. Bilmes, *A gentle tutorial on the EM algorithm and its application to parameter estimation for Gaussian mixture and hidden Markov models.*, Technical Report, University of Berkeley, ICSI-TR-97-021, 1997., 1997.
10. C. M. Bishop, *Neural networks for pattern recognition.*, Oxford University Press, 1995.
11. A. K. Jain and P. W. Duin, "Statistical pattern recognition: a review.," *IEEE Transactions on Pattern Anaysis and Machine Intelligence* **22**(1), pp. 4–37, 2000.
12. J. J. Oliver, R. A. Baxter, and C. S. Wallace, "Unsupervised learning using MML.," in *Proceedings of ICML-1996*, pp. 364–372, Morgan Kaufmann Publishers, (Bari, Italy), June 3–6 1996.
13. C. S. Wallace and D. L. Dowe, "Minimum message length and Kolmogorov complexity.," *The Computer Journal* **42**(4), pp. 270–283, 1999.
14. A. R. Barron, J. Rissanen, and B. Yu, "The minimum description length principle in coding and modeling.," *IEEE Transactions on Information Theory* **44**(6), pp. 2743–2760, 1998.
15. J. Rissanen, *Stochastic complexity in statistical inquiry theory.*, World Scientific Publishing Co., Inc., River Edge, NJ, USA, 1989.
16. H. Akaike, "A new look at the statistical model identification.," *IEEE Transactions on Automatic Control* **19**, pp. 716–723, 1974.
17. A. Lanterman, "Schwarz, Wallace, and Rissanen: Intertwining themes in theories of model order estimation.," *International Statistical Review* **69**, pp. 185–212, 2001.
18. M. A. T. Figueiredo and A. K. Jain, "Unsupervised learning of finite mixture models.," *IEEE Transactions on Pattern Analysis and Machine Intelligence* **24**(3), pp. 381–396, 2002.
19. A. Papoulis, *Probability & statistics.*, Prentice-Hall International, Englewood Cliffs, 1990.
20. M. Kass, A. Witkin, and D. Trezopoulos, "Snakes: active contour models.," *International Journal of Computer Vision* **1**(4), pp. 321–331, 1988.
21. T. McInerney and D. Terzopoulos, "Deformable models in medical images analysis: a survey.," *Medical Image Analysis* **1**(2), pp. 91–108, 1996.
22. C. Xu and J. L. Prince, "Generalized gradient vector flow external forces for active contours.," *Signal Processing* **71**(2), pp. 131–139, 1998.
23. C. Xu and J. L. Prince, "Snakes, shapes, and gradient vector flow.," *IEEE Transactions on Image Processing* **7**(3), pp. 359–369, 1998.
24. A. K. Jain, Y. Zhong, and M.-P. Dubuisson-Jolly, "Deformable template models: a review.," *Signal Processing* **71**(2), pp. 109–129, 1998.
25. L. D. Cohen, "On active contour models and balloons.," *Computer Vision, Graphics and Image Processing: Image understanding* **53**(2), pp. 211–218, 1991.
26. T. Aach, A. P. Condurache, K. Eck, and J. Bredno, "Statistical-model based identification of complete vessel-tree frames in coronary angiograms.," in *Electronic Imaging 2004: Computational Imaging II*, **5299**, pp. 283–294, SPIE, (San Jose, CA, USA), January 18–22 2004.